Catalysis Today 148 (2009) 179–183

Contents lists available at ScienceDirect

Catalysis Today

journal homepage: www.elsevier.com/locate/cattod

Morphology-dependent redox and catalytic properties of CeO_2 nanostructures: Nanowires, nanorods and nanoparticles

Tana [a,b], Milin Zhang [a], Juan Li [b], Huaju Li [b], Yong Li [b], Wenjie Shen [b,*]

[a] College of Material Science and Chemical Engineering, Harbin Engineering University, Harbin 150001, China
[b] State Key Laboratory of Catalysis, Dalian Institute of Chemical Physics, Chinese Academy of Sciences, 457 Zhongshan Road, Dalian 116023, China

ARTICLE INFO

Article history:
Available online 26 March 2009

Keywords:
Nanomaterials
CeO_2
Catalysts
Redox
Morphology-dependence

ABSTRACT

The redox features and the catalytic activities of ceria nanowires, nanorods and nanoparticles were comparatively studied. The morphology-dependent phenomenon is closely related to the nature of the exposed crystal planes. The CeO_2 nanoparticles mainly expose the stable {1 1 1} plane on the surface, whereas the rod-shaped nanostructures preferentially expose the reactive {1 1 0} and {1 0 0} planes, giving higher oxygen storage capacity and catalytic activity for CO oxidation. Although both the CeO_2 nanorods and the CeO_2 nanowires predominantly expose the reactive {1 1 0} and {1 0 0} planes, the CeO_2 nanowires favor to expose a large proportion of active planes on the surface, resulting in a much higher activity for CO oxidation than the nanorods.

1. Introduction

Cerium dioxide (CeO_2) has been extensively studied and applied in heterogeneous catalysis based on its ability to release and uptake oxygen under operation conditions with preserving the fluorite crystal structure [1,2]. It is commercially an important component of the three-way catalysts (TWCs) for automotive exhaust gas control. Ceria acts as an oxygen buffer by absorbing and releasing oxygen through a fast Ce^{3+}/Ce^{4+} cycle in the TWCs, and simultaneously promotes the oxidation of CO to CO_2, involving the participation of the lattice oxygen species [1]. This unique redox property is usually described by the oxygen storage capacity (OSC), which is largely dependent on the size of ceria particles [1–3]. In addition to the particle size, however, the morphology also influences the redox feature of ceria significantly, depending on the exposed crystalline planes [4,5]. One-dimensional ceria nanostructures such as nanorods [4–6], nanowires [7] and nanotubes [8,9] have been synthesized successfully and examined for catalytic reactions. For example, CeO_2 nanorods which predominantly expose the reactive {1 1 0} and {1 0 0} planes showed significantly enhanced activity for CO oxidation than the ceria nanoparticles that mainly expose the less reactive {1 1 1} plane [4].

The typical CeO_2 nanoparticle is mainly composed of polyhedron which exposes eight {1 1 1} or eight {1 1 1} and six {1 0 0} planes, but the rod-shaped nanostructures tend to preferentially expose four {1 1 0} and two {1 0 0} planes [4,5]. Therefore, the oxygen storage of CeO_2 nanoparticles is confined mainly on the surface, while the oxygen species both on the surface and in the bulk could participate in the redox cycle in the nanorods, giving a much higher oxygen storage capacity. In fact, it has been readily confirmed that the oxygen storage capacity (in terms of exposed crystal planes) of ceria follows the order of nanocubes > nanorods ≫ nanopolyhedra, implying that the low-indexed plane has a higher OSC [5]. It seems that the rod-shaped ceria nanomaterials could show significantly enhanced redox property by predominantly exposing the reactive planes and thus the well-defined active sites for catalytic reactions might be achieved by controlling the morphologies of ceria nanostructures.

In this work, we report a comparative study on the redox features and the catalytic activities of ceria nanomaterials, including nanowires, nanorods and nanoparticles. The morphology-dependent effect of the ceria nanomaterials is closely related to the nature of the exposed crystal planes.

2. Experimental

2.1. Synthesis of CeO_2 nanomaterials

CeO_2 nanowires and nanorods were synthesized by a hydrothermal process through varying the initial concentrations of the reactants and the hydrothermal period. An appropriate amount of $Ce(NO_3)_3{\cdot}6H_2O$ (0.86 g for nanowires, 3 g for nanorods) and NaOH (16 g for nanowires, 6.4 g for nanorods) were dissolved into 80 ml distilled water. The solution was then transferred to an autoclave (100 ml) and gradually heated to 373 K and kept at this temperature for 24 h (nanowires) and 14 h (nanorods). The solid

* Corresponding author. Tel.: +86 411 84379085; fax: +86 411 84694447.
E-mail address: shen98@dicp.ac.cn (W. Shen).

0920-5861/$ – see front matter © 2009 Elsevier B.V. All rights reserved.
doi:10.1016/j.cattod.2009.02.016

obtained was washed with hot water, dried at 373 K over night and finally calcined at 673 K for 4 h in air. The yields of the nanorods and nanowires were around 80%.

The CeO_2 nanoparticles were prepared by precipitating ammonia cerium nitrate with urea in aqueous solution, as described elsewhere [10]. Briefly, 60 g of $(NH_4)_2Ce(NO_3)_6$ and 200 g of urea were dissolved into 2000 ml of distilled water and the mixture was heated gradually to 363 K under stirring and kept at this temperature for 27 h. After filtration and being washed with water, the precipitate was dried at 373 K for 12 h, and finally calcined at 673 K for 5 h in air.

2.2. Characterization

Powder X-ray diffraction (XRD) patterns of the samples were recorded on a Rigaku D/Max-RB diffractor with Cu Kα radiation (λ = 0.15418 nm). The crystalline size of the ceria nanoparticle was calculated from the Scherrer equation with the FWHM of the (1 1 1) plane.

N_2 adsorption–desorption isotherms were recorded at 77 K using a Nova 4200e instrument. Before the measurement, the sample was degassed at 573 K for 2 h. The specific surface area was calculated by the BET equation.

Transmission electronic microscopy (TEM) images were recorded on a FEI Tecnai G^2 Spirit microscope with an accelerating voltage of 120 kV, and high resolution transmission electronic microscopy (HRTEM) images were obtained on a FEI Tecnai G^2 F30 S-Twin microscope at an acceleration voltage of 300 kV. Specimens were prepared by ultrasonically suspending the powder sample in ethanol. A drop of the suspension was deposited on a thin carbon film supported standard copper grid and dried in air.

Hydrogen temperature-programmed reduction (H_2-TPR) was performed with a U-type quartz reactor equipped with a thermal conductivity detector (TCD). 100 mg samples (40–60 mesh) were loaded and pretreated with a 20%O_2/He mixture (30 ml/min) at 423 K for 1 h and cooled to room temperature under N_2 flow. The samples were then heated to 1173 K at a rate of 10 K/min under the flow of a 5%H_2/N_2 mixture (30 ml/min). After cooling to 673 K in He flow, pulses of oxygen were injected periodically and the OSC was estimated from the total quantity of oxygen consumed.

CO temperature-programmed desorption (CO-TPD) was conducted with a U-shape quartz reactor coupled to a mass spectrometer (OMNI Star Balzers). 100 mg samples were pretreated with a 20%O_2/He mixture (30 ml/min) at 423 K for 1 h and then cooled to 323 K in He flow. After exposing to a mixture of 10%CO/He (30 ml/min) for 0.5 h and being purged with He, the sample was heated to 673 K at a rate of 10 K/min under He flow (30 ml/min).

2.3. Catalytic evaluation

CO oxidation was conducted in a continuous flow fixed-bed quartz reactor under atmospheric pressure. 200 mg samples were loaded and pretreated with a 20%O_2/He mixture (30 ml/min) at 423 K for 1 h. After cooling to room temperature, the reactant gas (1%CO/21%O_2/He, 30 ml/min) was then introduced and the temperature was programmed to rise at a rate of 10 K/min. The composition of outlet gas was on-line analyzed by gas chromatogram.

3. Results and discussion

Fig. 1 shows the XRD patterns of the CeO_2 nanomaterials. Typical diffraction peaks of ceria fluorite structure (JCPDS 34-0394) are observed for all the samples. The nanowires and nanorods exhibit relatively higher crystallinity than the nanoparticles. The BET areas of the nanowires, nanorods and nanoparticles are 130, 128 and 155 m^2/g, respectively. The crystalline size of the ceria nanoparticle is about 6 nm.

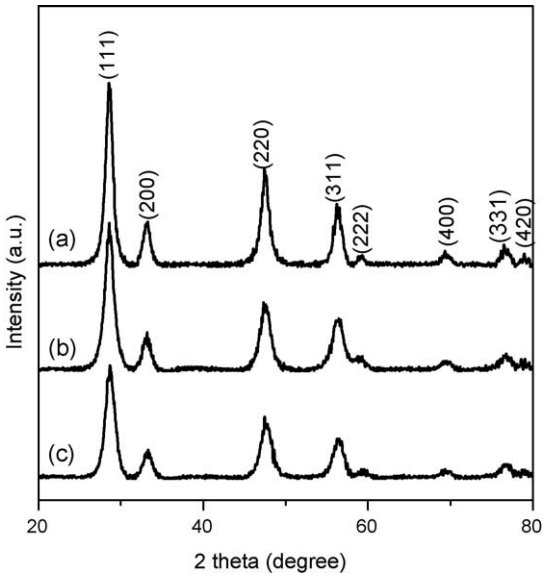

Fig. 1. XRD patterns of the CeO_2 nanowires (a), nanorods (b) and nanoparticles (c).

Fig. 2 shows the TEM images of the CeO_2 nanomaterials. The CeO_2 nanoparticles have an average size of about 6 nm, and the projection of the nanoparticle shows a hexagonal shape, indicating that the nanoparticles are composed of truncated octahedral. When viewed along the [1 1 0] direction, the interplanar spacing of 0.31 nm indicates the dominant presence of the {1 1 1} plane. The nanorods are 7–15 nm in lateral size and 60–120 nm in longitudinal, and the average diameter and length are 11 and 100 nm, respectively. When viewed along the [1 0 0] direction, the lattice spacing of the fringes perpendicular to the elongation direction of the nanorod is 0.19 nm, showing that the CeO_2 nanorods prefer to expose the {1 1 0} and {1 0 0} planes, in accord with previous observations [4,5,11]. The nanowires have the average diameter of about 7 nm and the average length of around 140 nm, giving a higher aspect ratio of 20 than the nanorods. Judged from the interplanar spacing and the plane-intersecting angles, the nanowires seem to grow along the [1 1 0] direction and to expose the {1 1 0} and {1 0 0} planes mainly.

Fig. 3 shows the H_2-TPR profiles of the CeO_2 nanomaterials. All the samples exhibit a broad reduction peak at 510–910 K and a high-temperature reduction peak above 1000 K. It is generally accepted that the low-temperature reduction is due to the removal of surface oxygen and the high-temperature reduction is related to the oxygen species in bulk ceria [1]. The intense low-temperature reduction peak in the nanoparticles indicates that the amount of hydrogen consumed is larger than those of the nanowires and nanorods. This observation is consistent with the trend of the specific surface area. In general, ceria materials with higher surface area and smaller particle size tend to have more crystal edges and corners, which in turn produce higher concentration of surface oxygen species. On the other hand, the rod-shaped ceria materials often have higher crystallinity and larger crystal size, resulting in a lower concentration of surface oxygen species.

The real redox property of ceria can be measured indirectly by TPR with followed re-oxidation, as suggested by previous studies [4,12,13]. Therefore, the oxygen storage capacities of the ceria nanomaterials were measured at 673 K by oxygen titration after the TPR processes. As shown in Table 1, the OSC is 735, 557 and 538 μmol O_2/g for the nanowires, nanorods and nanoparticles, respectively. Moreover, the specific OSC (divided by the surface area) of the rod-shaped ceria is still larger than that of the particles.

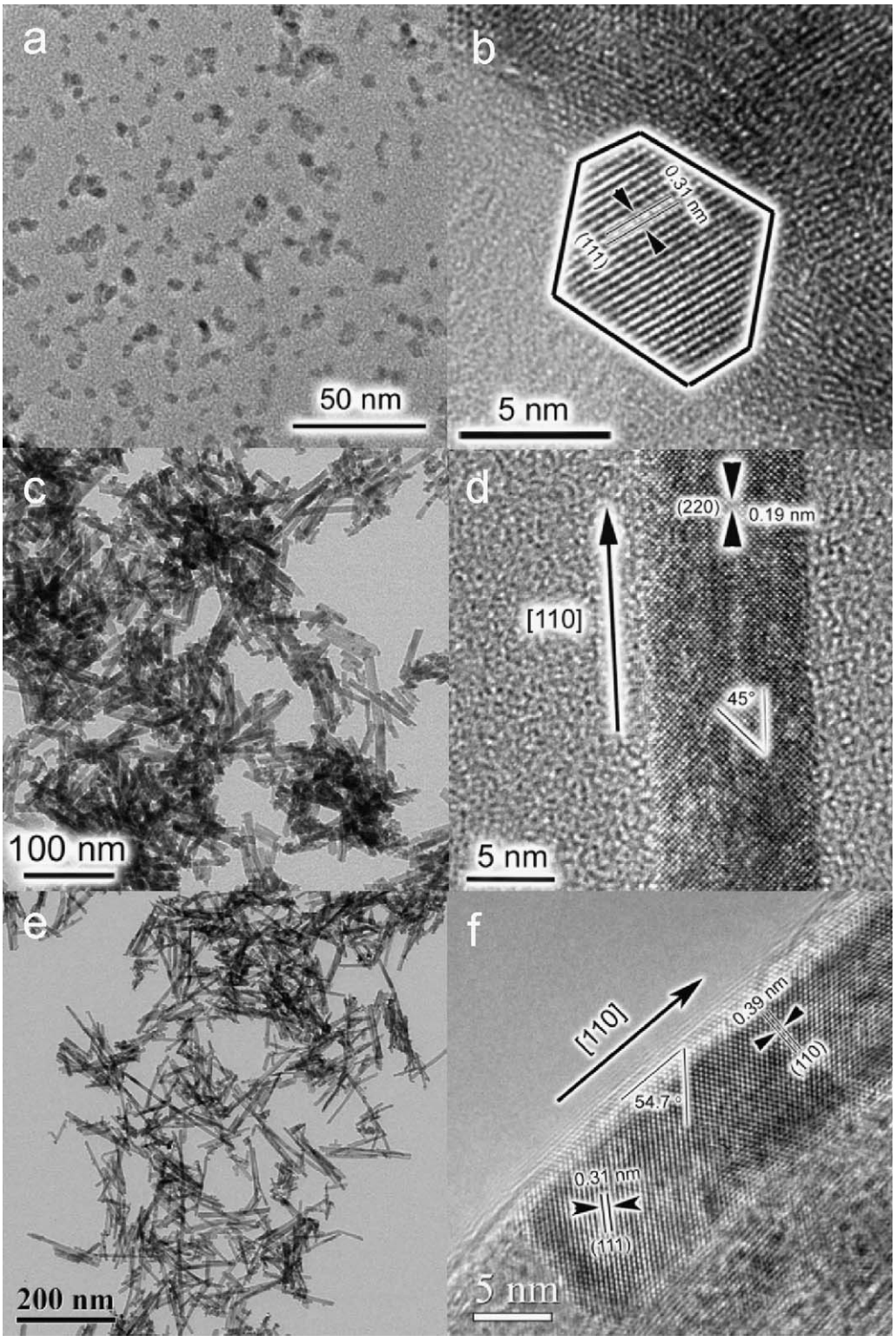

Fig. 2. TEM images of the CeO_2 nanoparticles (a and b), nanorods (c and d) and nanowires (e and f).

This phenomenon demonstrates that the real OSC of the CeO_2 nanomaterials depends strongly on the morphology. The significant loss in the redox property of the nanoparticles might be caused by the decrease of surface area through aggregation [12] and/or the reconstruction of the fine clusters occurred under the reducing atmosphere with increasing temperature [4,14,15].

It was previously confirmed that the CeO_2 nanorods could show enhanced redox property than the nanoparticles because of the dominant exposure of reactive {1 0 0} and {1 1 0} planes [4,5]. However, the CeO_2 nanowires here exhibit a much higher OSC than the nanorods despite their comparable specific surface area and similar geometrical configuration. Probably, the proportion of the {1 1 0} and/or {1 0 0} planes exposed on the surface varies between the nanorods and the nanowires. Since the OSC on the (1 0 0) plane is much higher than that on the (1 1 0) plane in CeO_2 [15], it is most likely that the nanowire exposes relatively more {1 0 0} planes on

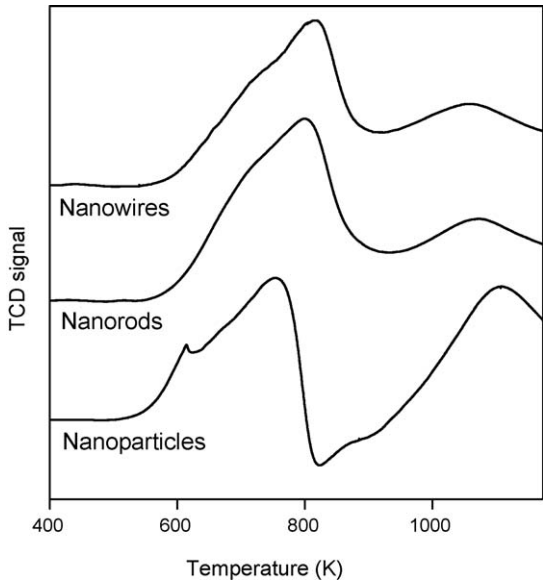

Fig. 3. H_2-TPR profiles of the CeO_2 nanomaterials.

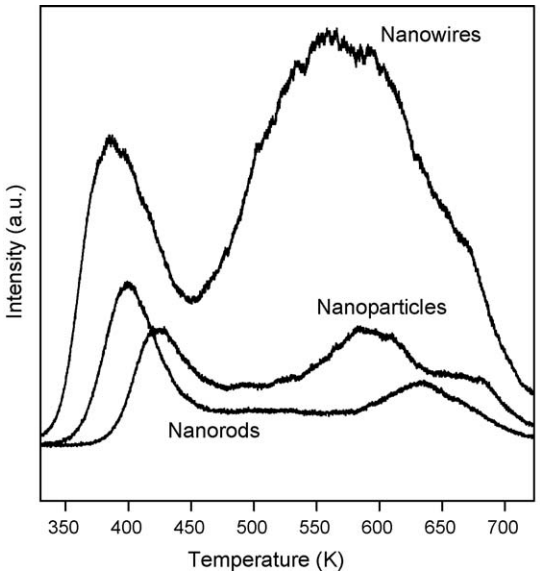

Fig. 4. CO-TPD profiles of the CeO_2 nanomaterials.

Table 1
Exposed crystal planes, OSCs, and surface areas of the CeO_2 nanomaterials.

Sample	Nanowires	Nanorods	Nanoparticles
Exposed planes	{1 1 0} + {1 0 0}	{1 1 0} + {1 0 0}	{1 1 1} + {1 0 0}
OSC (μmol O_2/g)	735	557	538
S_{BET} (m^2/g)	130	128	155

the surface than the nanorod, although both of them preferentially expose the {1 1 0} and {1 0 0} planes. Another possibility comes from the higher aspect ratio of the nanowire. As mentioned above, the average diameter and length of the nanorod are 11 and 100 nm, respectively, whereas the nanowire has the average diameter of 7 nm and the average length of 140 nm. Both of them grow along the [1 1 0] direction, the reactive {1 0 0} and {1 1 0} planes are preferentially exposed on the surfaces. However, the proportion of these active planes in the nanowire is relatively higher than that in the nanorod, mainly because of the smaller diameter and the larger length.

Fig. 4 shows the CO-TPD profiles of the CeO_2 nanomaterials. Desorption of CO_2 is observed for all the samples, indicating that the pre-adsorbed CO is fully oxidized into CO_2 by the oxygen species in ceria. Especially, significant desorptions of CO_2 appear at around 383 and 560 K on the CeO_2 nanowires, evidencing that there are more adsorption sites for CO. Both theoretical simulation and experimental measurement for CO adsorption on ceria have revealed that only weak adsorption is present on the {1 1 1} plane, while weak and strong adsorptions co-exist on the {1 1 0} plane and only strong adsorption occurs on the {1 0 0} plane [15–18]. Since the CeO_2 nanowires mainly expose the {1 1 0} and {1 0 0} planes, the formation of CO_2 at 383 K might be related to the adsorbed CO on the {1 1 0} plane, whereas the CO_2 evolution at 560 K is mainly caused by the strong adsorption of CO on the {1 0 0} plane. Therefore, it seems that both the nanorods and the nanowires dominantly expose the {1 1 0} and {1 0 0} planes, but the nanowires expose a large proportion of these active planes on the surface.

Fig. 5 shows the catalytic activities of the CeO_2 nanomaterials for CO oxidation. It is obvious that the CeO_2 nanowires are more active than the CeO_2 nanorods and nanoparticles, particularly in the low-temperature region. At 533 K, the conversion of CO is about 70% on the nanowires, whereas it is only 38% over the nanoparticles. The light-off temperature (T_{90}), the temperature at which 90% conversion of CO is achieved, is around 573 K on the nanowires, which is 20 K lower than that on the nanoparticles. Apparently, the superior catalytic performance of the CeO_2 nanowires is closely related to the unique morphology, which preferentially exposes the reactive {1 0 0} and {1 1 0} planes.

It is generally accepted that the oxidation of CO to CO_2 on ceria involves the participation of lattice oxygen species [1,19], and thus the CeO_2 nanorods which predominantly expose the active {1 1 0} and {1 0 0} planes show significantly enhanced activity for CO oxidation than the CeO_2 nanoparticles that mainly expose the less reactive {1 1 1} plane [4]. Theoretical calculations further confirmed that the reactivity for CO oxidation on the surface planes follows the order of (1 0 0) > (1 1 0) > (1 1 1) [20–22]. Since the

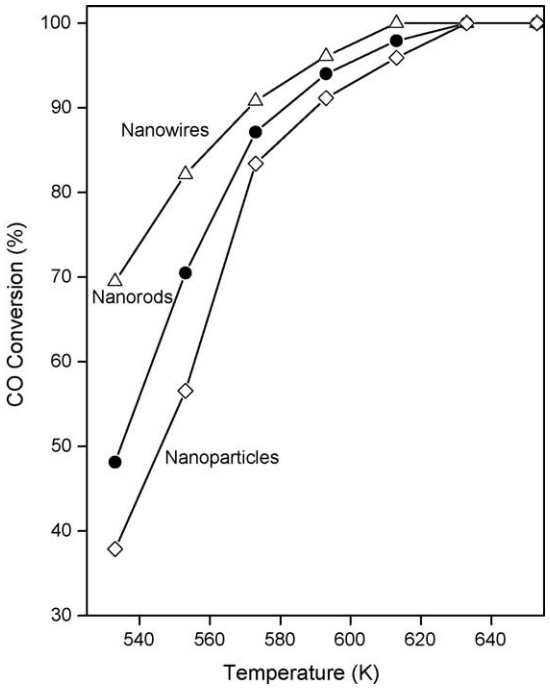

Fig. 5. CO conversions over the CeO_2 nanomaterials. Reaction conditions: 200 mg catalyst, 1%CO/21%O_2/He, 30 ml/min.

CeO_2 nanorods/nanowires predominantly expose the reactive {1 1 0} and {1 0 0} planes while the CeO_2 nanoparticles mainly expose the most stable {1 1 1} planes, it is reasonable that the CeO_2 nanorods/nanowires are more active than the CeO_2 nanoparticles. Although both the CeO_2 nanorods and the CeO_2 nanowires predominantly expose the reactive {1 1 0} and {1 0 0} planes, the CeO_2 nanowires expose a large proportion of these active planes on the surface as judged from the TEM observation and OSC/TPD measurements. As a result, the CeO_2 nanowires exhibit much higher activity for CO oxidation than the nanorods.

4. Conclusions

CeO_2 nanowires presented a higher catalytic activity for CO oxidation and oxygen storage capacity than the nanorods, although both of them were more reactive than the nanoparticles. Both the CeO_2 nanorods and the CeO_2 nanowires predominantly expose the reactive {1 1 0} and {1 0 0} planes, but the CeO_2 nanowires favor to expose a large proportion of these active planes on the surface, resulting in a much higher activity for CO oxidation than the nanorods.

References

[1] A. Trovarelli, Catal. Rev. Sci. Eng. 38 (1996) 439.
[2] A. Trovarelli, Catalysis by Ceria and Related Materials, Imperial College Press, London, 2002.
[3] S. Carrettin, P. Concepción, A. Corma, J.M. Nieto, V.F. Puntes, Angew. Chem. Int. Ed. 43 (2004) 2538.
[4] K.B. Zhou, X. Wang, X.M. Sun, Q. Peng, Y.D. Li, J. Catal. 229 (2005) 206.
[5] H.X. Mai, L.D. Sun, Y.W. Zhang, R. Si, W. Feng, H.P. Zhang, H.C. Liu, C.H. Yan, J. Phys. Chem. B 109 (2005) 24380.
[6] C. Pan, D. Zhang, L. Shi, J. Fang, Eur. J. Inorg. Chem. 15 (2008) 2429.
[7] N. Bugayeva, J. Robinson, Mater. Sci. Technol. 23 (2007) 237.
[8] K.B. Zhou, Z.Q. Yang, S. Yang, Chem. Mater. 19 (2007) 1215.
[9] W.Q. Han, L.J. Wu, Y.M. Zhu, J. Am. Chem. Soc. 127 (2005) 12814.
[10] W. Cai, B. Zhang, Y. Li, Y. Xu, W. Shen, Catal. Commun. 8 (2007) 1588.
[11] N. Du, H. Zhang, B. Chen, X. Ma, D. Yang, J. Phys. Chem. C 111 (2007) 12677.
[12] D. Terribile, A. Trovarelli, C. de Leitenburg, G. Dolcetti, Chem. Mater. 9 (1997) 2676.
[13] E.S. Putna, J.M. Vohs, R.J. Gorte, J. Phys. Chem. 100 (1996) 17862.
[14] H. Cordatos, D. Ford, R.J. Gorte, J. Phys. Chem. 100 (1996) 18128.
[15] Y. Madier, C. Descorme, A.M. Le Govic, D. Duprez, J. Phys. Chem. B 103 (1999) 10999.
[16] D.R. Mullins, S.H. Overbury, J. Catal. 188 (1999) 340.
[17] Z.X. Yang, T.K. Woo, K. Hermansson, Chem. Phys. Lett. 396 (2004) 384.
[18] M. Nolan, G.W. Watson, J. Phys. Chem. B 110 (2006) 16600.
[19] H.C. Yao, Y.F. Yu Yao, J. Catal. 86 (1984) 254.
[20] T.X.T. Sayle, S.C. Parker, C.R.A. Catlow, Surf. Sci. 316 (1994) 329.
[21] D.C. Sayle, S.A. Maicaneanu, G.W. Watson, J. Am. Chem. Soc. 124 (2002) 11429.
[22] Z. Yang, T.K. Woo, M. Baudin, M.K. Hermansson, J. Chem. Phys. 120 (2004) 7741.